Design of Multiple Space Debris Removal Missions using Machine Learning

Giulia VIAVATTENE[1a], Ellen DEVEREUX[b], David SNELLING[b], Niven PAYNE[b], Stephen WOKES[c], Matteo CERIOTTI[a]

[a] *James Watt School of Engineering, University of Glasgow, G12 8QQ, Glasgow, United Kingdom*
[b] *Fujitsu UK, W1U 3BW, London, United Kingdom*
[c] *Astroscale, Harwell Science Park, OX11 0QG, Oxford, United Kingdom*

Abstract

Active debris removal (ADR) allows for the disposal of inactive satellites and larger objects, preventing the build-up of space junk and allowing to replace aging agents in a constellation. To make ADR missions more commercially viable, the removal and disposal of multiple debris objects using a single spacecraft are investigated. This paper proposes the use of artificial neural networks (ANNs) to quickly estimate the cost and duration of the transfers to de-orbit a range of debris objects, so that it is possible to identify the optimal sequence of objects which minimizes the cost and/or the duration of the mission, for the maximum number of de-orbited objects. To this end, the ANN is integrated within a sequence search algorithm based on a tree search. The performance of the proposed methodology is assessed by analyzing three distinctive sequences of multiple space debris removals. A near-term low-thrust propulsion technology enables to dispose of up to 13 debris objects within 10 years, when the optimal design parameters are chosen. The use of ANN allows for this solution to be found 26 times faster than current methods, while enabling the selection of faster and less expensive (being the propellant mass required lower) options.

Keywords: Space Debris, Debris Removal, Artificial Neural Network, Machine Learning, Astrodynamics, Low thrust

1. Introduction

Active debris removal (ADR) is the process to dispose inactive objects from space, preventing the build-up of junk, such as non-functional spacecraft, abandoned launch vehicle stages and other large objects, and replace faulty agents in satellite constellations [1, 2]. ADR can be particularly useful for those larger debris objects that would not de-orbit naturally in a short timeframe (for example due to their altitude), or those which may pose a threat to active satellites; collisions of larger objects also cause a sudden growth of the debris population due to fragmentation, which could eventually lead to the *Kessler syndrome* [3, 4]. ADR is currently being investigated and demonstrator missions are being designed and flown. The RemoveDEBRIS mission, led by the University of Surrey, is a satellite research project to demonstrate various space debris removal technologies for ADR (e.g., net and harpoon capture) [5]. The ADR demonstration mission ELSA-d was launched by Astroscale in April 2021 to test the magnetic capture mechanism which they have developed, and it is currently in orbit.[2] Also, the European Space Agency (ESA) with its CleanSpace initiative is looking at the required technology developmentsx to capture debris. The ClearSpace-1 mission aims at de-orbiting a Vega upper stage by 2025.[3] Interest is also emerging in the removal of multiple debris objects in a single ADR mission [6, 7]. This can provide significant advantages not only from a financial prospective, but also from a timing prospective, especially in cases where it is necessary to remove multiple objects within a

[1] Corresponding author: g.viavattene.1@research.gla.ac.uk

[2] `https://astroscale.com/astroscale-celebrates-successful-launch-of-elsa-d/`

[3] `https://www.esa.int/Safety_Security/Clean_Space/ESA_commissions_world_s_first_space_debris_removal`

limited time frame [2, 8]. This study proposes a new methodology which uses machine learning techniques to efficiently design missions for the disposal of multiple debris objects using a single spacecraft (referred to as the *chaser* throughout the paper). This approach can reduce the overall launch cost and significantly reduce the computational time involved during the design phase.

In this work, it is assumed that several debris objects are tracked and identified for disposal. A subset of them is selected in an ordered sequence, based on the transfer cost and duration to reach and de-orbit them, for the ADR mission. The ADR mission profile involves the chaser to rendezvous and dock with the first debris object in the sequence, and lower the perigee altitude to a drag-dominated region, i.e., to a disposal low Earth orbit (LEO), where the object is released for de-orbiting and re-entry. Then, the chaser transfers to the next target object and the procedure repeats until the propellant is depleted. A schematic representation of the mission scenario is provided in Figure 1, where Di with $i = 1, 2, ...$ indicates each of the debris objects located at different altitudes and $\Delta\Omega$ is the difference in right ascension of the ascending node between debris orbits.

It is worth noting that, when the debris object is released in a low-altitude disposal orbit, the debris will re-enter by spiraling down due to atmospheric drag [9]. Re-entries of large debris objects shall be controlled and aiming at uninhabited areas, such as the South Pacific Ocean Uninhabited Area (SPOUA). Semi controlled reentries are currently under study as they could allow de-orbitation with low thrust in the future.

The purpose of this study is to find sequences of debris objects to be disposed of from a given set, and design multiple ADR missions which are optimal in terms of propellant mass consumption (or equivalently ΔV). To this end, the following challenges need to be addressed. First, the selection of the debris objects to be disposed of, and their sequence, shall be identified so that the overall trajectory cost is minimized. Second, the orbital transfers between a debris orbit and the disposal orbit, and vice-versa, shall be designed so that the required propellant mass (m_{prop}) and/or time-of-flight (TOF) are minimized. It should be stressed that two problems cannot be solved independently of each other, because the first one, which is combinatorial, requires various inputs, such as duration and cost of each transfer, which are obtained by solving the second problem, and vice-versa.

Rendezvousing and de-orbiting multiple debris objects in a single mission is highly demanding in terms of energy. For this reason, an efficient propulsion system is required to keep the propellant mass ratio low. A low-thrust technology, such as the solar electric propulsion (SEP) system, is a good candidate because of its high specific impulse [10, 11].

To identify the best sequence of objects, all the combinations of debris should be explored and evaluated. Above 80% of the trackable objects in near-Earth space are space debris.[4][5] Scientific models estimate the total number of space debris objects in Earth orbit to be in the order of 36,000 for sizes larger than 10 cm, 990,000 for sizes larger than 1 cm, and more than 135 millions for sizes larger than 1 mm. The selection of space debris to remove should account for the size of the debris, the collision risk with active satellites, the availability of useful orbital slots, and the type of capture mechanism.

Considering just the largest objects as candidates for removal [12], billions of permutations would need to be investigated to identify the most convenient ADR mission. Since trajectory optimization, and specifically low-thrust transfers, are notoriously computationally demanding, we propose to use machine learning, allowing for a significant reduction of the computational time.

In the past, machine learning was applied successfully to solve complex problems in aerospace sciences. Artificial neural networks (ANNs) were employed by Dachwald (2004) [13], Hennes et al. (2016) [14] and Mereta et al. (2017) [15] to compute the low-thrust trajectories to asteroids, demonstrating that machine learning techniques can explore the trajectory space search more exhaustively than traditional optimal control methods. Other applications include the accurate computation of pinpoint landing [16] and orbit prediction [17]. ANNs were successfully used in the preliminary design of multiple asteroid rendezvous missions [18–20].

[4] `www.space-track.org`, visited on 25 September 2021

[5] `www.ucsusa.org/resources/satellite-database`, visited on 25 September 2021

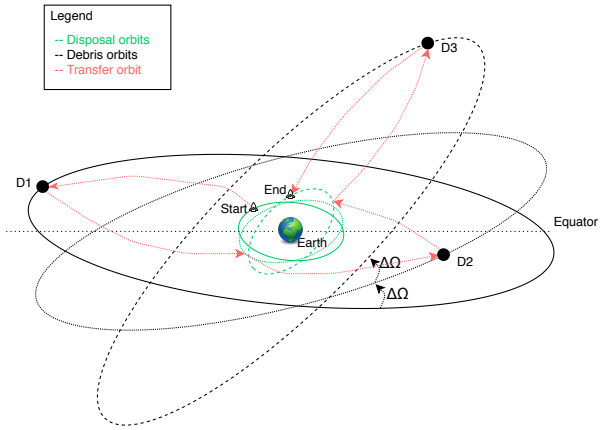

Figure 1: Schematic representation of the mission scenario.

The goal of this study is to provide a method for a fast optimization of ADR missions for multiple debris removal, when numerous candidate objects are available. An ANN is trained to quickly estimate the cost of a trajectory in terms of m_{prop} and TOF, given the debris orbits, so that the most effective sequences of debris to be disposed of can be identified. The ANN is integrated within a sequence search algorithm which computes the feasible debris sequences. The candidate sequences which minimize the objective function (e.g., m_{prop} and/or TOF) can be selected and further refined through optimal control problem solvers.

The paper is organized as follows. Section 2 describes the dynamics of the system. The ANN design is detailed in Section 3, where the generation of the training database is also discussed. In Section 4, the sequence search algorithm is described and the logic is explained. Three debris sequences with minimum cost, which are identified by the sequence search and ANN (SS-ANN) platform, are analyzed and the performance of the proposed methodology assessed. Finally, Section 5 provides a summary of the methodology and the findings.

2. Dynamics of the System

To identify the mission plan for the multiple debris removals, the propellant mass and duration of each of the listed phases need to be estimated. In this section, the dynamics of the system is presented, where the chaser is modeled as a point mass with continuous low-thrust.

The dynamics of the spacecraft and debris objects are described and propagated using modified equinoctial elements [21]: p the semi-latus rectum, f and g the elements describing the eccentricity, h and k the elements describing the inclination, and L the true longitude. This avoids numerical singularities for zero eccentricity and inclination of the classical Keplerian elements.

The dynamics of the space objects can be described using the following differential equation:

$$\dot{\mathbf{x}}(t) = \mathbf{A}(\mathbf{x})\mathbf{a} + \mathbf{b}(\mathbf{x}) \tag{1}$$

where the state vector $\mathbf{x}$ is defined by the modified equinoctial elements, i.e., $\mathbf{x} = (p, f, g, h, k, L)$, $\mathbf{a}$ is the perturbing acceleration in radial, transversal, out-of-plane components, and $\mathbf{A}(\mathbf{x})$ and $\mathbf{b}(\mathbf{x})$ are the matrix and the vector of the dynamics, respectively. The matrix $\mathbf{A}(\mathbf{x})$ can be fully formulated as follows [22]:

$$\mathbf{A} = \begin{bmatrix} 0 & a_{1,2} & 0 \\ a_{2,1} & a_{2,2} & a_{2,3} \\ a_{3,1} & a_{3,2} & a_{3,3} \\ 0 & 0 & a_{4,3} \\ 0 & 0 & a_{5,3} \\ 0 & 0 & a_{6,3} \end{bmatrix} \tag{2}$$

where:

$$a_{1,2} = \frac{2p}{q}\sqrt{\frac{p}{\mu}} \tag{3a}$$

$$a_{2,1} = \sqrt{\frac{p}{\mu}}\sin(L) \tag{3b}$$

$$a_{2,2} = \sqrt{\frac{p}{\mu}}\frac{1}{q}\left((q+1)\cos(L) + f\right) \tag{3c}$$

$$a_{2,3} = -\sqrt{\frac{p}{\mu}}\frac{g}{q}\left(h\sin(L) - k\cos(L)\right) \tag{3d}$$

$$a_{3,1} = \sqrt{\frac{p}{\mu}}\cos(L) \tag{3e}$$

$$a_{3,2} = \sqrt{\frac{p}{\mu}}\frac{1}{q}\left((q+1)\sin(L) + g\right) \tag{3f}$$

$$a_{3,3} = \sqrt{\frac{p}{\mu}}\frac{f}{q}\left(h\sin(L) - k\cos(L)\right) \tag{3g}$$

$$a_{4,3} = \sqrt{\frac{p}{\mu}}\frac{s^2\sin(L)}{2q} \tag{3h}$$

$$a_{5,3} = \sqrt{\frac{p}{\mu}}\frac{s^2\cos(L)}{2q} \tag{3i}$$

$$a_{6,3} = \sqrt{\frac{p}{\mu}}\left(h\sin(L) - k\cos(L)\right) \tag{3j}$$

while the vector $\mathbf{b}(\mathbf{x})$ can be fully formulated as follows [22]:

$$\mathbf{b} = \begin{bmatrix} 0 \\ 0 \\ 0 \\ 0 \\ 0 \\ \sqrt{\mu p}\left(\frac{q}{p}\right)^2 \end{bmatrix} \tag{4}$$

where

$$q = 1 + f\cos(L) + g\sin(L) \tag{5}$$

$$s^2 = 1 + \chi^2 \tag{6}$$

$$\chi = \sqrt{h^2 + k^2} \tag{7}$$

2.1. Perturbing Accelerations

The perturbing acceleration, $\mathbf{a}$, is given by (i) the acceleration due to the thrust $\mathbf{a_T}$, (ii) the acceleration due to the oblateness of the Earth $\mathbf{a_g}$ and (iii) the acceleration due to atmospheric drag $\mathbf{a_D}$, i.e.:

$$\mathbf{a} = \mathbf{a_T} + \mathbf{a_g} + \mathbf{a_D} \tag{8}$$

The motion of the debris objects are also propagated starting from given initial conditions considering the same dynamics with gravitational and atmospheric perturbations (but no thrust).

2.1.1. Thrust

The acceleration on the chaser spacecraft due to the thrust $\mathbf{a_T}$ is given as:

$$\mathbf{a_T} = \frac{T_{max}}{m}\mathbf{N} \tag{9}$$

where T_{max} is the maximum thrust that the propulsion system can generate, m is the mass of the system (chaser and, if docked, debris object) and $\mathbf{N} = [N_r, N_\theta, N_h]^T$ indicates the acceleration direction and magnitude vector in radial, transverse, and out-of-plane coordinates. The mass of the system m decreases with time due to the propellant consumption as described by the following mass differential equation:

$$\dot{m} = -\frac{T_{max}|\mathbf{N}|}{I_{sp}g_e} \tag{10}$$

where $|\mathbf{N}|$ is the magnitude of $\mathbf{N}$, which accounts for the thrust throttling, I_{sp} is the specific impulse of the propulsion system and $\mathbf{g_e}$ the gravitational acceleration at the Earth's surface. The propulsive acceleration is provided by the chaser spacecraft only.

2.1.2. Non-spherical Gravitational Acceleration

The gravitational acceleration is experienced by both the chaser and debris objects, due to the Earth's oblateness, and generally mass density distribution, can be defined as follows [23]:

$$\mathbf{a_g} = \mathbf{Q_r^T}\delta\mathbf{g} \tag{11}$$

where $\mathbf{Q_r} = [\mathbf{i_r}\mathbf{i}_\theta\mathbf{i_h}]$ is the transformation matrix from the rotating local-vertical-local-horizontal frame to the Earth-centered inertial (ECI) frame, whose components are:

$$\mathbf{i_r} = \frac{\mathbf{r}}{||\mathbf{r}||}, \qquad \mathbf{i}_\theta = \mathbf{i_h} \times \mathbf{i_r}, \qquad \mathbf{i_h} = \frac{\mathbf{r} \times \mathbf{v}}{||\mathbf{r} \times \mathbf{v}||} \tag{12}$$

with $\mathbf{r}$ and $\mathbf{v}$ being, respectively, the position and velocity vectors of the spacecraft in the ECI frame. The perturbation acceleration $\delta\mathbf{g}$ is formulated as:

$$\delta\mathbf{g} = \delta g_n \mathbf{i_n} - \delta g_r \mathbf{i_r} \tag{13}$$

where $\mathbf{i_n}$ is the local north direction:

$$\mathbf{i_n} = \frac{\mathbf{e_n} - (\mathbf{e_n^T}\mathbf{i_r})\mathbf{i_r}}{||\mathbf{e_n} - (\mathbf{e_n^T}\mathbf{i_r})\mathbf{i_r}||} \tag{14}$$

and

$$\delta g_n = -\frac{\mu\cos(\phi)}{r^2}\sum_{k=2}^{n}\left(\frac{R_e}{r}\right)^k P'_k(\sin(\phi))J_k \tag{15}$$

$$\delta g_r = -\frac{\mu}{r^2}\sum_{k=2}^{n}(k+1)\left(\frac{R_e}{r}\right)^k P_k(\sin(\phi))J_k \tag{16}$$

Table 1: Constants and system parameters.

Constant	Value
g_e	9.8066 m/s^2
μ	$3.9860 \cdot 10^{14}$ m^3/s^2
R_e	$6378.14 \cdot 10^3$ m
J_2	$1082.639 \cdot 10^{-6}$
J_3	$-2.565 \cdot 10^{-6}$
J_4	$-1.608 \cdot 10^{-6}$
Parameter	**Value**
T_{max}	21 mN
I_{sp}	2000 s
m_0	400 kg
C_D	2.2
S	8 m^2

with $\mathbf{e_n} = [0, 0, 1]$, R_e the equatorial radius of the Earth, $r = p/q$, $P_k \sin(\phi)$ representing the k-th degree Legendre polynomial whose derivative with respect $\sin(\phi)$ is $P'_k \sin(\phi)$, and J_k being the zonal harmonic coefficient for $k = \{2, 3, 4\}$.

2.1.3. Atmospheric Drag

The acceleration due to the atmospheric drag in the radial, transverse and normal components can be defined as:

$$\mathbf{a_D} = [a_{D_r} \quad a_{D_\theta} \quad 0] \tag{17}$$

where the out-of-plane component of $\mathbf{a_D}$ is negligible, as the net plane change is close to zero. The radial and transverse components are defined as follows:

$$a_{D_r} = -0.5\rho S C_D v v_r \tag{18}$$

$$a_{D_\theta} = -0.5\rho S C_D v v_\theta \tag{19}$$

where ρ is the atmospheric density, which can be estimated using the *Exponential Atmospheric Model* [24]. Also, S is the aerodynamic surface area, C_D is the drag coefficient and v is the velocity magnitude, with v_r and v_θ being its radial and tangential components:

$$v_r = \sqrt{\frac{\mu}{p}} \left(f \sin(L) - g \cos(L)\right) \tag{20}$$

$$v_\theta = \sqrt{\frac{\mu}{p}} \left(1 + f \cos(L) + g \sin(L)\right) \tag{21}$$

The numerical values of the physical parameters, which are used in this study, are detailed in Table 1.

2.2. Transfer Model

Current satellite constellations are often on circular orbits, at the same inclination and spaced in RAAN. However, they might be at different altitude, for example, due to malfunctioning of the thruster or to the depletion of their fuel and hence started to de-orbit. For this reason, this work uses a set of debris objects on circular orbits at the same inclination; thus, the rendezvous transfers to and from space debris objects require the chaser to match the altitude and right ascension of the ascending node Ω (RAAN) of the orbit of the arrival body (Debris 2, or D2) at the arrival epoch, while departing from the departure body (Debris 1, or D1). Additionally, the phasing along the orbit between the chaser and debris is neglected in the transfer

model. The low-thrust transfer legs exhibit a large number of revolutions, thus the correct phasing can be attained with minimal propulsive effort, and often with little additional transfer time. These assumptions are chosen to keep the transfer model simple to minimize the computational time of the training database, and demonstrate the ANN capabilities. However, they are representative of a real mission and, therefore, they can be easily varied for future use-cases.

In order to minimize the propellant consumption and guarantee that a larger number of debris can be disposed for the given propellant mass, it is chosen to use the thrust to obtain the change in altitude and to exploit the Earth's oblateness gravitational perturbation (J_2) to achieve the change in Ω through *RAAN-phasing orbits*. The orbital-averaged RAAN variation rate is given by the Gauss equations as follows [25]:

$$\dot{\Omega} = -\left[\frac{3}{2}\frac{J_2\sqrt{\mu}R^2}{a^{7/2}(1-e^2)^2}\cos(i)\right] \tag{22}$$

which is experienced by both the chaser and the debris objects.

As shown in Figure 1, the mission scenario requires multiple orbital transfers for the chaser to rendezvous each debris object and transfer it into the disposal orbit (which is circular and at the same inclination of the debris objects' orbits). This suggests an iterative procedure, starting from a state where the chaser is docked to D1, where each iteration comprises of:

- A de-orbiting transfer from D1's orbit to the disposal orbit (with duration T_1), for releasing of the object
- A transfer from the disposal orbit to the most convenient RAAN-phasing orbit (with duration $T_{2,a}$)
- A RAAN-phasing orbit (with duration T_p)
- A transfer from the phasing orbit to D2's orbit (with duration $T_{2,b}$)
- A stay time at D2's orbit, for rendezvous and docking operations (with duration T_s)

Given the initial RAAN of D1 and D2, $\Omega_{1,0}$ and $\Omega_{2,0}$, and their RAAN variation rate, $\dot{\Omega}_1$ and $\dot{\Omega}_2$, respectively, it is possible to compute the RAAN of D2, $\Omega_{2,f}$, and of the chaser, $\Omega_{SC,f}$, at time t_f when the chaser is rendezvousing D2:

$$\Omega_{2,f} = \Omega_{2,0} + \dot{\Omega}_2(T_1 + T_2 + T_p) \tag{23}$$

$$\Omega_{SC,f} = \Omega_{1,0} + \dot{\Omega}_{T1}T_1 + \dot{\Omega}_{T2}T_2 + \dot{\Omega}_p T_p \tag{24}$$

where $T_2 = T_{2,a} + T_{2,b}$, and $\dot{\Omega}_{T1}$, $\dot{\Omega}_{T2}$ and $\dot{\Omega}_p$ are the RAAN variation rates experienced by the chaser along T_1, T_2 and T_p, respectively.

For the chaser to match the D2's orbit, we require that $\Omega_{2,f} = \Omega_{SC,f}$, and this can be solved for the RAAN-phasing time T_P:

$$T_P = \frac{\Delta\Omega_P}{\dot{\Omega}_P + \dot{\Omega}_2} \tag{25}$$

where $\Delta\Omega_P = \Omega_{1,0} + \dot{\Omega}_{T1}T_1 + \dot{\Omega}_{T2}T_2 + \Omega_{2,0} + \dot{\Omega}_2\,(T_1 + T_2)$.

As an example, Fig. 2 shows the changes in altitude, RAAN, burn maneuvers and mass as function of time for the full transfer from D1 ($h_{D_1} = 504.96$ km, $\Omega_{D_1} = 158.72$ deg, $m_{D_1} = 270.37$ kg) to D2 ($h_{D_2} = 1077.40$ km, $\Omega_{D_2} = 149.33$ deg, $m_{D_2} = 156.50$ kg). The chaser starts at altitude h_{D_1} with Ω_{D_1}, docked with D1, and carries it down to a disposal orbit and releases it. Once completed, the transfer to the next object starts, and chaser transfers to the RAAN-phasing orbit (which in this example coincides with the disposal orbit, thus $T_{2,a} = 0$ s). Once the chaser reaches the required RAAN, it transfers to D2's orbit by matching h_{D_2} and $\Omega_{D_{2,f}}$ (shown by the first subplot and second subplot). Finally, a fixed stay time,

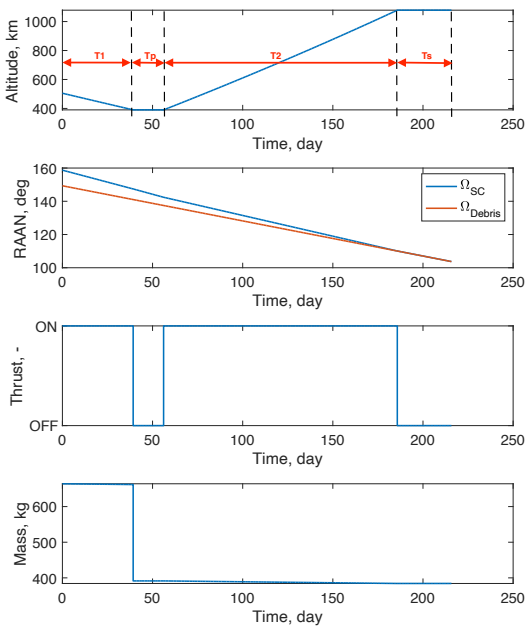

Figure 2: Transfer model.

$T_s = 30$ days (to allow for phasing and docking) is considered where the altitude is fixed and equal to h_{D_2}. Since during T_p and T_s there is no change in altitude, the thrust does not operate, as illustrate in the third subplot. The mass of the system (forth subplot), which comprises of chaser and D1's mass during T_1, drops at the end of T_1 when the debris object is released. Over time, the mass decreases due to thrusting during the transfers.

2.2.1. Thrust Model

The chaser's SEP system is powered by solar arrays which are subject to blackout periods during solar eclipse conditions. This causes a discontinuity in power (and thrust) available to the chaser, which needs to be taken into account in the thrust model.

In the eclipse model, for which a schematic representation is presented in Fig. 3, the Earth is assumed to be spherical and to project a cylindrical shadow region in the direction opposing the sun, within the equatorial plane. The shadow region is defined by the angle θ, which is the angle between the equator and the intersection of the edge of the eclipse and the orbit of the chaser. It is assumed that the chaser cannot thrust while traveling through the shadow region. To allow the tangential accelerations to change the orbit's semimajor axis with negligible change in eccentricity, it is required that the chaser thrusts along opposing arcs on the orbit. This also allows two duty cycles of the thruster per orbit. For these reasons, it is assumed that the chaser thrusts only outside of the two opposing arcs of angle 2θ indicated in Fig. 3.

To account for a suitable duty-cycle, the thrusters of the chaser are considered to be off for 40% of the time, which is assumed to be correspondent to when travelling through the shadow region. From this, the angle θ results equal to 36 deg, i.e., eclipse angle $2\theta = 72$ deg.

2.2.2. Optimal RAAN-Phasing Orbit

Considering the perturbing accelerations which act on the chaser and space debris continuously, the altitude of the RAAN-phasing orbit is chosen as a trade off between (i) time T_{PT} required to reach the phasing altitude and the phasing time and (ii) ΔV_{PT} to perform the change of altitude and the one required to counteract the drag action while phasing:

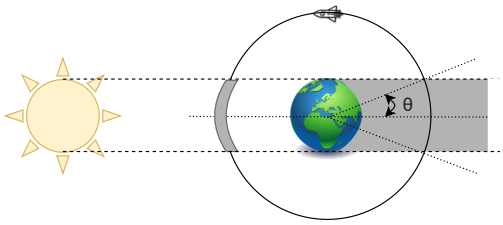

Figure 3: Eclipse model.

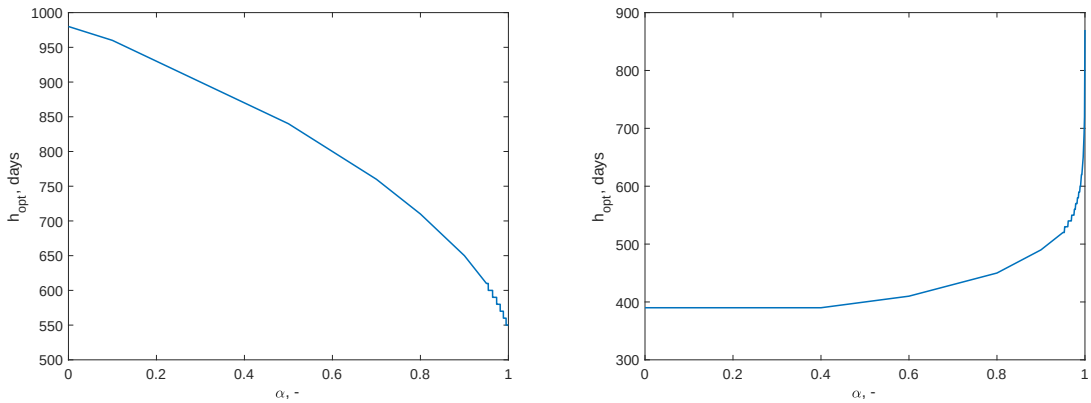

(a) $h_2 = 500$ km (b) $h_2 = 1000$ km

Figure 4: Optimal altitude h_{opt} as function of α when the arrival debris is located at a lower altitude or higher altitude.

$$\Delta V_{PT} = \Delta V_P + \Delta V_{d\to p} + \Delta V_{p\to D2} \tag{26}$$

$$T_{PT} = T_P + T_{d\to p} + T_{p\to D2} \tag{27}$$

where the indices P, $d \to p$ and $p \to D2$ indicate the RAAN-phasing orbit, the transfer from the disposal orbit to the phasing orbit, and the transfer from the phasing orbit to D2, respectively. The minimum altitude of the phasing orbit is set to be the disposal altitude.

The objective function used for the selection of the optimal phasing altitude can be defined as follows:

$$J = \alpha \Delta V_{PT} + (1-\alpha) T_{PT} \tag{28}$$

with $\alpha \in [0, 1]$ being a weighting factor which can be chosen be the mission designer, compromising between propellant mass and time of flight.

Figures 4, 5 and 6 show how the optimal altitude, the phasing time T_P and ΔV_P due to the drag, T_{PT} and ΔV_{PT} vary for different values of α chosen by the mission designer, respectively. It can be noticed that these variations also depend on the altitude of the arrival debris, in this case a lower altitude of 500 km shown in subfigures (a) and a higher altitude of 1000 km in subfigures (b) (with $\Delta\Omega$ around 360 deg). Shorter phasing time is generally required when the difference in altitude between the phasing and D2 orbit is maximized in order to match the RAAN of the arrival debris quicker. In case of low altitude of D2, it is convenient to wait at higher orbit. However, Figure 4 shows that there is a maximum altitude above which it becomes inconvenient to wait due to the longer transfer time to reach those altitudes. The ΔV due to the drag is smaller for higher phasing orbits, however reaching higher altitudes may require additional ΔV due to longer transfers.

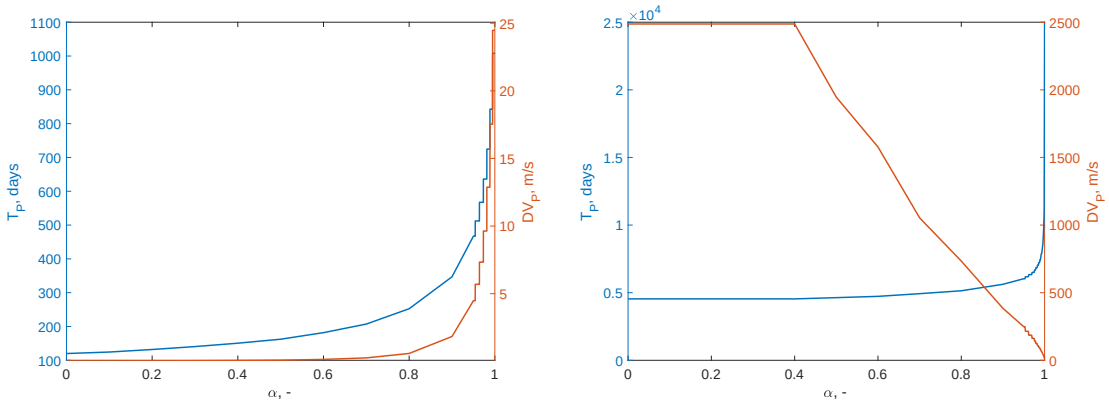

(a) $h_2 = 500$ km (b) $h_2 = 1000$ km

Figure 5: T_P and ΔV_P due to the drag as function of α when the arrival debris is located at a lower altitude or higher altitude.

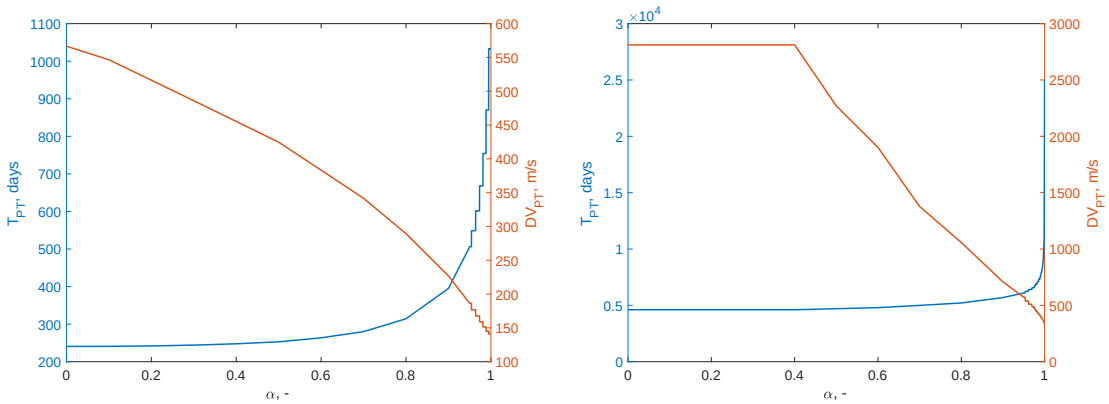

(a) $h_2 = 500$ km (b) $h_2 = 1000$ km

Figure 6: T_{PT} and ΔV_{PT} as function of α when the arrival debris is located at a lower altitude or higher altitude.

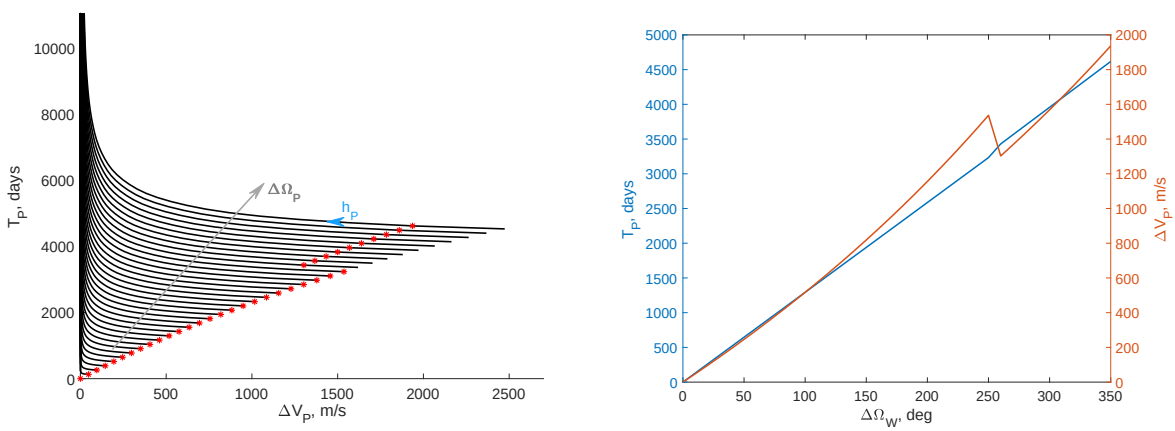

(a) Increasing h_P (b) At $h_{P,opt}$

Figure 7: T_P and ΔV_P as function of $\Delta\Omega$ for increasing phasing altitude and at the optimal altitude ($h_2 = 1000$ km, $\alpha = 0.5$).

It is noticed that Figures 4, 5 and 6 are highly dependent on the characteristics of the debris objects. For instance, if the objects are in an near-optimal RAAN-phasing condition after the orbital transfers, it can be more convenient to stay for a short amount of time at the disposal orbit to achieve the optimal RAAN instead of transferring to RAAN-phasing orbit with altitude higher than the one of D2 (as Figure 4(a) would suggest for lower altitudes).

Once the chaser reaches the target debris orbit of D2, a fixed capture time of 30 days is considered where the altitude is equal to D2's altitude to allow for the orbital phasing and capture operations to take place.

Figure 7(a) shows the variation of the phasing time T_P and the ΔV_P due to the drag on the phasing orbit, while increasing its altitude h_P, as a function of the $\Delta\Omega_P$ raising from 0 to 360 deg ($h_2 = 1000$ km, $\alpha = 0.5$). As h_P increases, T_P increases exponentially, with lower phasing orbit being preferred to maximize the difference between the RAAN variation rates at h_P and h_2. For larger $\Delta\Omega_P$, the curve shifts towards higher values of T_P and ΔV_P. In this plot, the red markers indicate the values of T_P and ΔV_P at the optimal phasing orbit $h_{P,opt}$. Figure 7(b) describes T_P and ΔV_P as function of $\Delta\Omega_P$ at the optimal altitude $h_{P,opt}$. As expected, while $\Delta\Omega_P$ increases, both the phasing time and the ΔV_P due to the drag increase almost linearly. However, ΔV_P presents a discontinuity at $\Delta\Omega_P = 250$ deg because over this value it is more convenient to phase at a slightly higher altitude ($h_P = 400$ km) than the disposal altitude as the reduction in ΔV_P is preferred over the marginally lower phasing time.

3. ANN for Multiple Debris Removal

Multi-layered feedforward ANNs can approximate any non-linear mapping $\mathbf{y}_t = \mathbf{f}(\mathbf{x})$ to any degree of accuracy [26]. A feedforward ANN is structured in layers, each presenting a number of neurons. The information travels from the input layer through the hidden layers to the output layer.

In order for the network to approximate the desired function (*network function*) appropriately, the network needs to be trained with a database containing the corresponding inputs and desired outputs (or targets). The network function is intended to minimize the network error, i.e., the mean square error (MSE) between the outputs generated by the network $\mathbf{y}$ and the targets $\mathbf{y}_t$:

$$\mathcal{E}_{MSE} = \frac{1}{N}\sum_{i=1}^{N} ||\mathbf{y}_i - \mathbf{y}_{t,i}||^2 \tag{29}$$

with N being the number of outputs.

3.1. Training Database

The training database contains the inputs and the desired outputs, which are used during the training of the network. The *input vector* $\mathbf{x}$ contains the orbital characteristics of the departure and arrival orbits, the mass of the departure debris m_{D1}, which needs to be carried to disposal, and the initial mass of the chaser m_{SC}, which varies during the mission due to the propellant consumption. The *output vector* $\mathbf{y}$ includes the propellant mass expenditure m_{prop}, which is related to ΔV by the Tsiolkovsky rocket equation, and the TOF $t_{0,f}$ of the transfer between the departure (D1) and arrival debris (D2). This yields:

$$\mathbf{x} = [h_{D1}, \Omega_{D1}, m_{D1}, h_{D2}, \Omega_{D2}, m_{SC}] \tag{30}$$

$$\mathbf{y} = [m_{prop}, t_{0,f}] \tag{31}$$

where h and Ω are the altitude and right ascension of the ascending node of the debris.

To generate the database 300 debris objects are considered, with altitudes between 500 and 1500 km with an inclination fixed to 87.9 deg, Ω between 0 and 360 deg, and mass between 100 and 300 kg. It should be noted that the most densely populated, thus critical, region in LEO is around 750–1000 km altitude with an inclination between 60 deg and 95 deg [8, 27]. Debris at other altitudes can be considered for removal for Space Traffic Management operation purposes. The disposal orbit is at an altitude of 390 km, which is also fixed. The chaser mass can vary from 300 kg to 400 kg, with the latter being the starting mass, since the on-board propellant mass is 100 kg. The training database comprises a total of 89,700 low-thrust transfers.

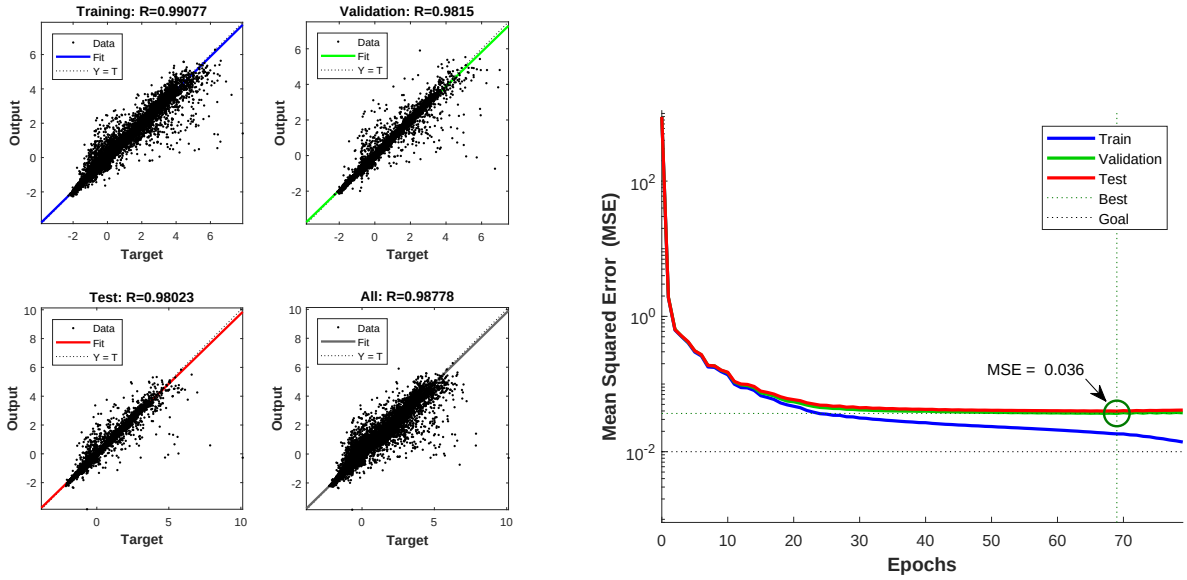

(a) Regression (b) Performance

Figure 8: ANN regression and performance analysis.

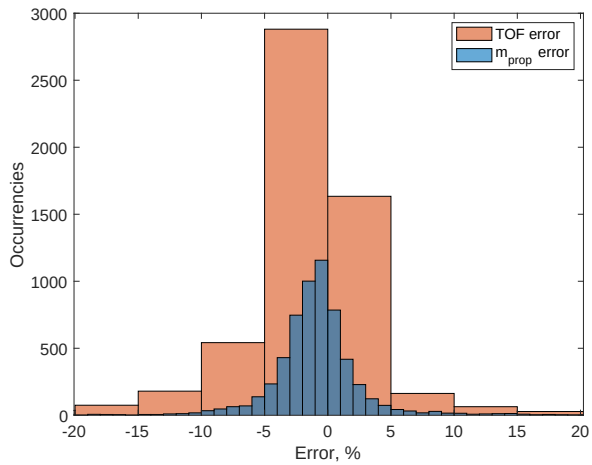

Figure 9: ANN error analysis.

For the training process the database is divided into three sets: training, validation and test. The training set is used to train the network. The validation set is used to eventually evidence the presence of overfitting during the training. The test set is used only after the training process to evaluate the final performance of the network. Since the validation set has samples which are not included in the training database, the validation-set MSE is often used as a performance indicator.

3.2. Performance Analysis

Figure 8 represents the performance of the trained network. The regression plot (a) shows how well the network outputs (Y-axis) fit the targets (X-axis) with respect to the training, validation, test sets and overall. A perfect fit, indicating an ideal performance of the network, is obtained when the data fall along

Table 2: Comparison of the proposed methodology SS-ANN against a current methods employed in the industry [28].

Method	No. Debris	No. Captures	Computational Time, min	Sequence	m_{prop}, kg	TOF, days
Industry	100	4	240	24, 1, 29, 54	30.7	2307
SS-ANN	100	4	9.37	44, 24, 38, 69	28.56	1559

the line with a unit slope and zero y-intercept, i.e., when the correlation R is 1. This means that the relationship between the outputs and the targets is $y = x$. The performance plot (b) shows how the MSE decreases during the training epochs until the performance goal is met. The final correlation achieved of 0.99 and the final validation-set MSE of 0.04 suggest a very accurate overall performance of the trained network.

An error analysis of the network output is performed and presented in Figure 9. The error is calculated as the mean percentage error between the output and the target, i.e.:

$$\mathcal{E}_y = \frac{1}{N} \sum_{i=1}^{N} \frac{y_i - y_{t,i}}{y_{t,i}} \cdot 100 \tag{32}$$

where y can be either the propellant mass or the time of flight. The maximum error experienced is of around $\pm 10\%$ and $\pm 20\%$ for m_{prop} and TOF, respectively, with a mean value of 1.27% and 4.02%. The performance and error analyses suggest that the training of the network was successful, thus the network can predict the propellant mass expenditure and TOF to dispose a sequence of debris with a high accuracy.

4. Sequence Search and Results

The following sequence search (SS) algorithm is implemented to identify the most promising sequences of debris to rendezvous, dock and de-orbit. The logic of the algorithm is based on a tree-search method and breadth-first criterion, which is schematically illustrated in Fig. 10. Each node of the tree represents a trajectory and how one proceeds through its branches depends on the mission objective which, in this case, is the TOF and m_{prop} minimization.

A database of $N = 5000$ fictitious debris objects is generated. Objects are a randomly created set with random mass $m_D \in [100, 300]$ kg, RAAN $\Omega_D \in [0, 360]$ deg and altitude $h_D \in [500, 1500]$ km. The SS works by selecting D_j as departure point and D_i as arrival point, with j and $i \in [1, N]$ so that all the possible permutations between objects can be evaluated. The trained ANN is embedded within the SS algorithm to calculate the m_{prop} and TOF of each low-thrust transfer. The $N_S = 100$ trajectories with the shorter transfer time are stored and a fixed capture time $t_{stay} = 30$ days is added at each object to ensure enough time for rendezvous and docking. At this point, the arrival object becomes the departure object of the following leg and the same procedure is iterated. The sequence is complete once the total mission duration exceeds 10 years (or until the depletion of the propellant mass).

In the following Sec. 4.1, the performance of the proposed methodology with the SS algorithm and the integrated ANN (SS-ANN) is assessed in terms of computational time, by comparing the results with those obtained through traditional methods. Then, in Sec. 4.2, the performance of the SS-ANN method is shown in term of the accuracy to identify the most convenient transfers and, thus, debris objects to de-orbit within a sequence.

4.1. Computational Time Analysis

The methodology SS-ANN is assessed, by comparing the performance with current methods employed in the industry [28], consisting of an industry expert processing the same input and providing the best solution possible within 4 hours via an iterative approach. For the comparison, the same set of input data (database of 100 debris objects with characteristics that are randomly generated, as mentioned above, number of captures and propellant system) and the same assumptions are used.

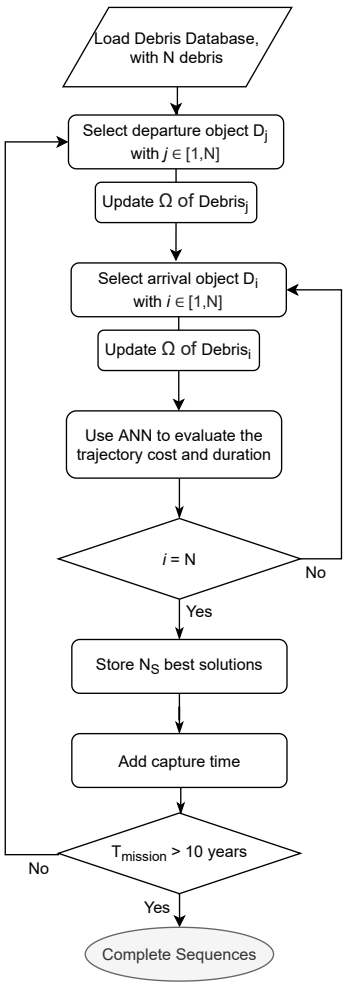

Figure 10: Sequence search algorithm.

Table 2 presents the results of this analysis. The sequence refers to the index of the objects from the database to be captured and the order in which they should be captured. For the same input data the computational time required by SS-ANN is more than 26 times faster than the time required for the current methods employed in the industry [28]. This result is obtained when 100 debris objects are considered, and it is expected that the benefits of using the SS-ANN method become even more important when a larger set of satellites is considered. Additionally, the m_{prop} and TOF found by the industry greatly exceed those found by the SS-ANN platform by 7% and 47%, respectively. It can be concluded that the benefits of the SS-ANN platform are not only in terms of the computational speed to select a solution, but also in terms of the optimality of the selected solution.

4.2. ADR Mission Design

To validate the outcome of the sequence search algorithm with a larger database of 5000 objects, the SS-AAN platform is run and three sequences are selected and their dynamics is fully solved for a SEP system with characteristics specified in Table 1. Three sequence searches are run for $\alpha = \{0, 0.95, 1\}$, and for each simulation the best sequence in terms of maximum number of debris objects disposed are selected.

Sequence A, obtained using $\alpha = 0$, allows for the disposal of 13 debris in 9.73 years with a required propellant mass of 84.97 kg. Sequence B, obtained using $\alpha = 0.95$, allows for the disposal of 11 debris in 10.87 years with a required propellant mass of 60.76 kg. Sequence C, obtained using $\alpha = 1$, allows for the

Table 3: Characteristics of the debris disposed in the selected sequences A ($\alpha = 0$), B ($\alpha = 0.95$) and C ($\alpha = 1$).

Seq. A	h, km	RAAN, deg	m, kg	m_{prop}, kg	$\mathcal{E}_{m_{prop}}$, %	TOF, days	$\mathcal{E}_{TOF}$, %
D1	637.16	287.50	163.40	N/A	N/A	N/A	N/A
D2	512.37	283	275.27	7.02	3.99	333.51	6.44
D3	585.17	275.30	138.41	5.26	4.58	188.44	8.89
D4	533.43	280.31	155.50	8.58	4.92	201.72	15.80
D5	644.38	256.52	212.14	7.14	6.79	398.12	6.37
D6	738.66	230.86	176.71	9.04	7.55	321.09	9.02
D7	501.13	274.57	106.99	7.34	3.35	251.63	3.86
D8	557.63	253.73	179.98	5.15	4.82	330.29	4.39
D9	516.09	259.77	105.56	5.82	8.27	347.93	5.66
D10	705.37	186.35	170.46	6.57	7.53	349.41	7.58
D11	588.68	221.62	191.09	7.61	1.87	290.43	7.05
D12	600.20	208.13	171.12	6.69	10.63	337.32	15.46
D13	526.06	244.28	175.02	8.74	8.37	205.03	1.37
Seq. B	h, km	RAAN, deg	m, kg	m_{prop}, kg	$\mathcal{E}_{m_{prop}}$, %	TOF, days	$\mathcal{E}_{TOF}$, %
D1	661.73	162.03	131.24	N/A	N/A	N/A	N/A
D2	504.96	158.72	270.37	6.63	9.77	311.92	10.41
D3	577.40	149.33	163.74	5.04	6.59	302.34	6.24
D4	534.05	145.48	256.27	6.35	3.73	517.09	3.88
D5	517.24	145.16	253.91	4.82	1.25	237.76	5.80
D6	514.14	138.62	139.19	6.02	7.03	460.15	3.59
D7	534.61	128.19	213.67	4.35	9.42	305.27	4.23
D8	667.95	84.76	222.82	5.21	1.40	95.18	8.00
D9	694.88	66.66	200.81	7.97	11.66	361.76	12.72
D10	517.45	123.32	171.80	9.39	9.77	768.67	6.66
D11	588.01	88.94	213.15	4.95	2.33	309.09	8.16
Seq. C	h, km	RAAN, deg	m, kg	m_{prop}, kg	$\mathcal{E}_{m_{prop}}$, %	TOF, days	$\mathcal{E}_{TOF}$, %
D1	533.43	280.31	155.50	N/A	N/A	N/A	N/A
D2	512.37	283	275.27	4.71	4.53	878.50	8.30
D3	585.17	275.30	138.41	5.07	10.86	1216.67	15.49
D4	543.71	288.64	172.30	5.33	4.43	1009.69	2.05
D5	517.31	303.68	291.92	4.93	5.25	960.91	7.10

disposal of 5 debris in 11.10 years with a required propellant mass of 20 kg. Figure 11 shows the change in altitude and propellant mass along the Sequences A, B and C.

As expected from the analysis of Figure 6, the choice of the weighting parameter α, thus of the phasing altitude, can have a significant impact on the propellant mass consumption and duration of the mission. As α increases, the TOF increases, while m_{prop} decreases. This is particularly noticeable for the case of $\alpha = 1$, when the TOF sharply raises compared to the cases of $\alpha = 0$ and 0.95, resulting in a sensible reduction of number of debris which can be de-orbited in about 10 years. Table 3 presents the characteristics (altitude h, RAAN, and mass m) of the space debris de-orbited as part of the Sequences A, B and C and the mission characteristics (propellant mass m_{prop} and TOF) of sequences obtained by solving the dynamics of the system.

Although for $\alpha = 1$, slightly less propellant mass is required to de-orbit a single debris (compared to, for example, the case of $\alpha = 0.95$), the duration of each transfer increases consistently. Overall, the modest reduction of used propellant mass does not seem to justify the steep increase in TOF. As also shown in

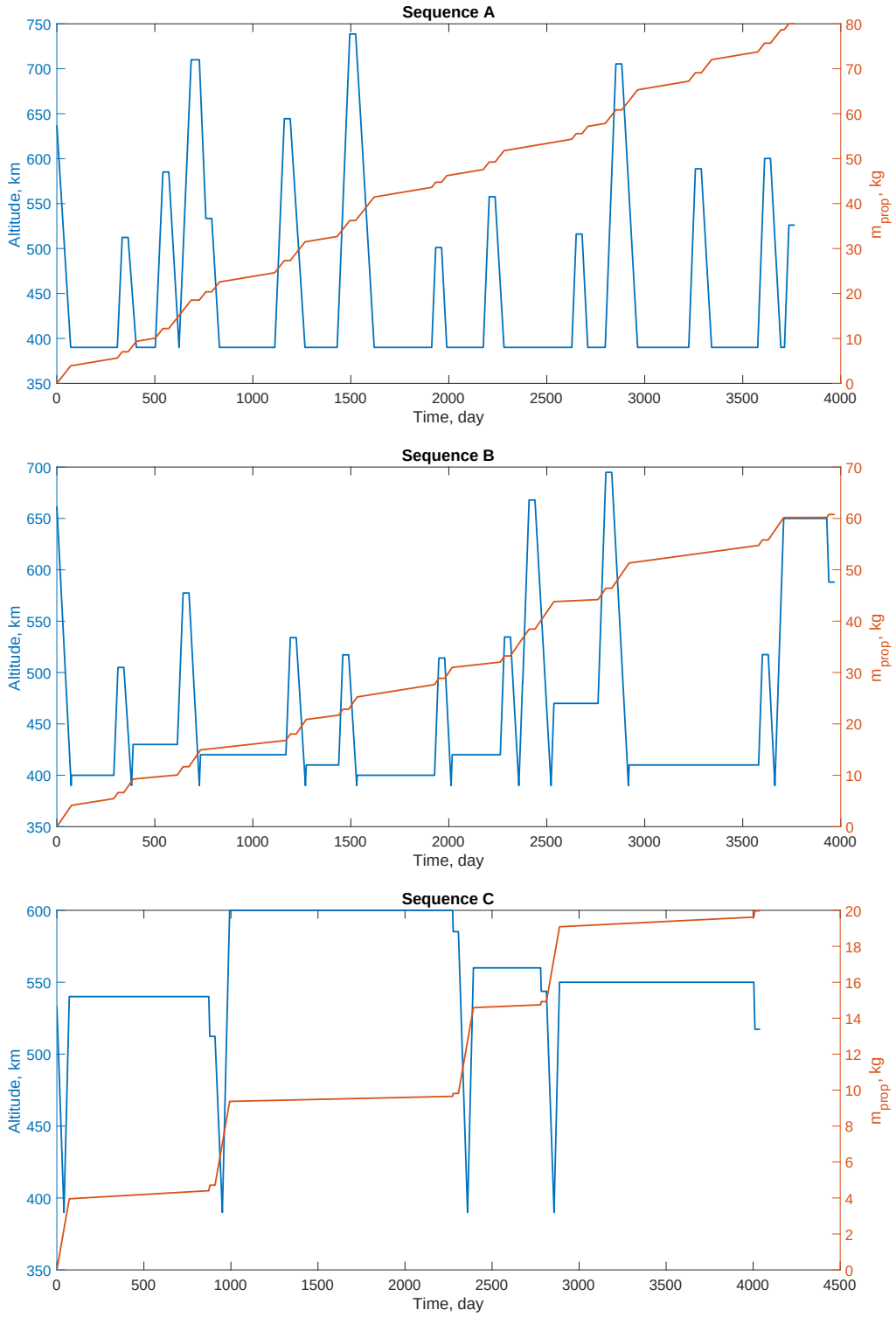

Figure 11: Altitude and propellant mass for sequences A, B and C.

Figure 6, varying the value of α between 0 and 0.95 allows to reduce the ΔV (and propellant mass) at the cost of a reasonable increase of TOF, while for $0.95 < \alpha < 1$ the TOF dramatically raises.

Table 3 also shows the percentage errors of three sequences between the values computed by the ANN and those obtained by solving the dynamics of the system. As expected, the percentage errors are generally lower that 10% for the propellant mass consumption and 15% for the TOF, with a final mean error of 6.04% for the m_{prop} estimation and 7.89% for the TOF estimation. It can be concluded that the trained network is able to estimate with reasonable accuracy the cost and duration of transfers to de-orbit space debris objects.

5. Conclusions

The proposed methodology uses an artificial neural network (ANN) to quickly estimate the cost and duration of low-thrust transfers for the disposal of multiple space debris. The ANN is trained with a training database of 90,000 samples and reaches a correlation of almost 0.99, which indicate an accurate performance. The network is integrated with a sequence search (SS) algorithm which, based on a tree-search method and and breadth-first criterion, can compute the most convenient sequences in terms of cost (i.e., propellant mass consumption) and duration of the mission.

The choice of the phasing altitude h_P has an impact on the final cost and duration of the mission and, consequently, on the number of debris which can be disposed in a given time frame. An objective function is defined to select the appropriate h_P, where the weighting factor α defines the trade-off between (i) the time required to reach the phasing altitude and the phasing time and (ii) the cost to perform the change of altitude and to counteract the drag action while phasing.

Three sequences have been selected to verify the performance of the proposed methodology. It is shown that up to 13 debris can be disposed of within 10 years while using less than 100 kg of the propellant mass, if the optimal RAAN-phasing orbit is selected.

Employing machine learning techniques within the sequence search algorithm (SS-ANN) greatly reduces the computational time by 26 times, when 100 debris are considered. The benefit derived from the speed of the algorithm increases further compared to traditional methods when a larger set of debris is considered. It is also shown that the SS-ANN methodology can select sequences which are shorter and less expensive (being the propellant mass required lower). Additionally, the proposed methodology ensures a high accuracy with an average percentage error of about 6.04% and 7.89% with respect to the target values of the propellant mass and time of flight.

It is important to underline that, despite the simple transfer model used in this work, selected to keep the computational time low, an ANN could be trained to estimate a more complex transfer model (i.e., with fully-optimal low-thrust legs) at the same cost in terms of computational time (after network training), which is a fraction of the time that a traditional optimizer would require.

6. Acknowledgments

Giulia Viavattene gratefully acknowledges the support received for this research from the James Watt School of Engineering at the University of Glasgow for funding the research under the James Watt sponsorship program.

The authors acknowledge the United Kingdom Space Agency (UKSA), for supporting part of this work.

References

[1] C. Bonnal, J. Ruault, M. Desjean, Active debris removal: recent progress and current trends, Acta Astronautica 85 (2013).

[2] J. Liou, A parametric study on using active debris removal for LEO environment remediation, Advances in Space Research 47 (11) (2011).

[3] D. J. Kessler, B. G. Cour-Palais, Collision frequency of artificial satellites: The creation of a debris belt, Advances in Space Research (1978) 2637–2646.

[4] D. McKnight, R. Witner, F. Letizia, S. Lemmens, L. Anselmo, C. Pardini, A. Rossi, C. Kunstadter, S. Kawamoto, V. Aslanov, J. Dolado Perez, V. Ruch, H. Lewis, M. Nicolls, L. Jing, S. Dan, W. Dongfang, A. Baranov, D. Grishko, Identifying the 50 statistically-most-concerning derelict objects in LEO, Acta Astronautica 181 (2021). doi:https://doi.org/10.1016/j.actaastro.2021.01.021.

[5] J. Forshaw, G. Aglietti, S. Fellowes, T. Salmon, I. Retat, et al, The active space debris removal mission RemoveDebris. Part 1: from concept to launch, Acta Astronautica 168 (2020). doi:10.1016/j.actaastro.2019.09.002.
[6] V. Braun, A. Lupken, S. Flegel, J. Gelhaus, M. Mockel, C. Kebschull, C. Wiedemann, P. Vörsmann, Active debris removal of multiple priority targets, Advances in Space Research 51 (9) (2013).
[7] N. Berend, X. Olive, Bi-objective optimization of a multiple-target active debris removal mission, Acta Astronautica 122 (2013).
[8] N. Van der Pas, J. Lousada, C. Terhes, M. Bernabeu, W. Bauer, Target selection and comparison of mission design for space debris removal by DLR's advanced study group, Acta Astronauta 102 (2014).
[9] J. Pollard, Bi-objective optimization of a multiple-target active debris removal mission, Joint Propulsion Conference and Exhibit, AIAA (1998). doi:10.2514/6.1998-3486.
[10] J. R. Wertz, Orbit & Constellation Design & Management, Springer, New York, 2009.
[11] R. G. Jahn, Physics of Electric Propulsion, McGraw-Hill Book Company, New York, 2006.
[12] Anselmo, L. and Pardini, C., Ranking upper stages in low Earth orbit for active removal, Acta Astronautica 122 (2016) 19–27.
[13] B. Dachwald, Optimization of interplanetary solar sailcraft trajectories, Journal of Guidance, Control, and Dynamics 27 (1) (2004). doi:10.2514/1.9286.
[14] D. Hennes, D. Izzo, D. Landau, Fast Approximators for Optimal Low-Thrust Hops Between Main Belt Asteroids, IEEE Symposium Series on Computational Intelligence (SSCI) (2016). doi:10.1109/SSCI.2016.7850107.
[15] A. Mereta, D. Izzo, A. Wittig, Machine Learning of Optimal Low-Thrust Transfers Between Near-Earth Objects, Hybrid Artificial Intelligent Systems (2017) 543–553doi:10.1007/978-3-319-59650-146.
[16] C. Sánchez-Sánchez, D. Izzo, Real-time optimal control via Deep Neural Networks: study on landing problems, Journal of Guidance, Control, and Dynamics 41 (3) (2018) 1122–1135. arXiv:1610.08668, doi:10.1023/B:CJOP.0000010527.13037.22.
URL http://arxiv.org/abs/1610.08668
[17] H. Peng, X. Bai, Artificial Neural Network–Based Machine Learning Approach to Improve Orbit Prediction Accuracy, AIAA Journal of Spacecraft and Rockets 55 (5) (2018) 1–13. doi:10.2514/1.A34171.
[18] G. Viavattene, M. Ceriotti, Artificial Neural Network for Preliminary Multiple NEA Rendezvous Mission Using Low Thrust, 70th International Astronautical Congress (IAC), Washington DC, USA (2019).
[19] G. Viavattene, M. Ceriotti, Low-thrust multiple asteroid missions with return to Earth using artificial neural networks, AAS/AIAA Astrodynamics Specialist Conference (2020).
[20] G. Viavattene, M. Ceriotti, Artificial neural network design for tours of multiple asteroids, Springer, Lectures Notes in Computer Science (2020). doi:10.1007/978-3-030-61705-9_63.
[21] J. T. Betts, Survey of Numerical Methods for Trajectory Optimization, Journal of Guidance, Control, and Dynamics 21 (2) (1998) 193–207. doi:10.2514/2.4231.
URL http://arc.aiaa.org/doi/10.2514/2.4231
[22] J. T. Betts, Practical Methods for Optimal Control and Estimation Using Nonlinear Programming, 2nd Edition, SIAM Press, Philadelphia, 2010.
[23] K. F. Wakker, Fundamentals Of Astodynamics, Faculty of Aerospace Engineering, Delft University of Technology, 2015.
[24] D. V. Schroeder, An Introduction to Thermal Physics, 3rd Edition, Addison-Wesley, 2000.
[25] H. Curtis, Orbital Mechanics for Engineering Students, Elsevier, 2005.
[26] I. Goodfellow, Y. Bengio, A. Courville, Deep Learning, The MIT Press, Cambridge, Massachusetts, 2016.
[27] J. Liou, Collision activities in the future orbital debris environment, Advances in Space Research 38 (2006) 2102—-2106.
[28] D. Snelling, E. Devereux, N. Payne, M. Nuckley, G. Viavattene, M. Ceriotti, S. Wokes, G. Di Mauro, H. Brettle, Innovation in Planning Space Debris Removal Missions Using Artificial Intelligence and Quantum-Inspired Computing, 8th European Conference on Space Debris, Darmstadt, Germany, 20-23 Apr (2021).